DOI: 10.6060/ivkkt.20256811.7165

УДК: 541.11

ПОЛУЧЕНИЕ ПОРИСТЫХ УГЛЕРОДНЫХ МАТЕРИАЛОВ И ИХ ЭЛЕКТРОКАТАЛИТИЧЕСКИЕ СВОЙСТВА ДЛЯ ВОССТАНОВЛЕНИЯ КИСЛОРОДА

Сунь Линтао, Цзинь Жун, Лиан Тан, Джунжи Жои, Т.Г. Черкасова, Чаоджонг Гао

Сунь Линтао (ORCID 0009-0002-5745-7450), Цзинь Жун (ORCID 0009-0006-9360-1973)

Школа научных материалов и инженерии, Чунцинский университет искусств и наук, Чунцин 402160, Китай
Кузбасский государственный технический университет, ул. Весенняя, 28, Кемерово, Российская Федерация, 650000
E-mail: 595118563@qq.com, 249109242@qq.com

Лиан Тан (ORCID 0009-0009-3491-2503), Джан Жоу (ORCID 0009-0003-3469-6632), Татьяна Григорьевна Черкасова (ORCID 0000-0002-5337-1337)*

Кузбасский государственный технический университет, ул. Весенняя, 28, Кемерово, Российская Федерация, 650000
E-mail: 1851611453@qq.com, ctg.htnv@kuzstu.ru*

Чаоджонг Гао (ORCID 0000-0002-3229-5777)

Школа научных материалов и инженерии, Чунцинский университет искусств и наук, Чунцин 402160, Китай
E-mail: guochaozhong1987@163.com

Хотя катализаторы на основе благородных металлов достигли превосходных показателей в реакциях восстановления кислорода на электродах (катодах) топливных элементов, дефицит, высокая стоимость и низкая долговечность этих металлических катализаторов затрудняют реализацию крупномасштабных применений. Цинк-кислородно-воздушная батарея – это экологически чистая батарея со многими преимуществами, такими как малый размер, малая масса, большой заряд, безопасность и надежность, а также она может поддерживать нормальную работу в широком диапазоне температур без коррозии. В данной статье основное внимание уделяется изучению легированных азотом углеродных материалов на основе железа. С помощью пиролиза и стратегий «хозяин-гость» были разработаны и проконтролированы морфология, структура и состав материалов для приготовления катализаторов OCB@g-C_3N_4 и катализаторов OCB-Hb@g-C_3N_4 с превосходной активностью в реакции восстановления кислорода (ORR), но и высокой стабильностью. Высокотемпературные карбонизированные материалы образуют покрытую углеродом структуру, которая закрепляет частицы железа в углеродном слое. Частицы железа присутствуют в форме носителей гемоглобина, синергически взаимодействуют с активными центрами для инициирования эффективных реакций восстановления кислорода. Поэтому оптимизация материала путем изменения температуры прокаливания может увеличить количество и экспозицию активного центра.

Ключевые слова: пористые углеродные материалы, реакция восстановления кислорода, катализатор, структурное регулирование

PREPARATION OF POROUS CARBON MATERIALS AND THEIR ELECTROCATALYTIC PROPERTIES FOR OXYGEN REDUCTION

Lingtao Sun, Rong Jin, Liang Tan, Junjie Zhou, T.G. Cherkasova, Chaozhong Guo

Lingtao Sun (ORCID 0009-0002-5745-7450), Rong Jin (ORCID 0009-0006-9360-1973)

School of Materials Science and Engineering, Chongqing University of Arts and Sciences, Chongqing 402160, China
T.F. Gorbachev Kuzbass State Technical University, str. Vesennyaya, 28, Kemerovo, 650000, Russia
E-mail: 595118563@qq.com, 249109242@qq.com

Liang Tan (ORCID 0009-0009-3491-2503), Junjie Zhou (ORCID 0009-0003-3469-6632), Tatiana G. Cherkasova (ORCID 0000-0002-5337-1337)*

T.F. Gorbachev Kuzbass State Technical University, Vesennyaya st., 28, Kemerovo, 650000, Russia
E-mail: 1851611453@qq.com, ctg.htnv@kuzstu.ru*

Chaozhong Guo (ORCID 0000-0002-3229-5777)

School of Materials Science and Engineering, Chongqing University of Arts and Sciences, Chongqing 402160, China
E-mail: guochaozhong1987@163.com

Although noble metal catalysts have achieved superior performance in fuel cell cathode oxygen reduction electrode reactions, the scarcity, cost and low durability of these metal catalysts make it difficult to carry out large-scale applications. Zinc-oxygen-air battery, is an environmentally friendly battery with many advantages such as small size, small mass, large charge, safety and reliability, and can maintain normal operation in a wide temperature range without corrosion. This paper focuses on the study of iron-based nitrogen-doped carbon materials. Through pyrolysis and host-guest strategies, the morphology, structure, and composition of the materials were designed and controlled to prepare OCB@g-C_3N_4 catalysts and OCB-Hb@g-C_3N_4 catalysts with excellent ORR (oxygen reduction reaction) activity and high stability. The high-temperature carbonized materials form a carbon-coated structure that anchors iron particles in the carbon layer. The iron particles are present in the form of hemoglobin carriers, which synergistically interact with active centers to initiate efficient oxygen reduction reactions. Electrochemical test results show that the synthesized catalysts not only have excellent ORR performance and long-term stability but also their outstanding ORR catalytic performance is determined by factors such as specific surface area, porous structure, appropriate graphitization, and degree of defects as revealed by physical characterization results. Therefore, optimizing the material by changing the calcination temperature can increase the number and exposure of active site.

Keywords: porous carbon materials, oxygen reduction reaction, catalyst, structural regulation

Для цитирования:
Сунь Линтао, Цзинь Жун, Лиан Тан, Джунжи Жои, Черкасова Т.Г., Чаоджонг Гао Получение пористых углеродных материалов и их электрокаталитические свойства для восстановления кислорода. *Изв. вузов. Химия и хим. технология*. 2025. Т. 68. Вып. 11. С. 87–95. DOI: 10.6060/ivkkt.20256811.7165.

For citation:
Lingtao Sun, Rong Jin, Liang Tan, Junjie Zhou, Cherkasova T.G., Chaozhong Guo Preparation of porous carbon materials and their electrocatalytic properties for oxygen reduction. *ChemChemTech [Izv. Vyssh. Uchebn. Zaved. Khim. Khim. Tekhnol.]*. 2025. V. 68. N 11. P. 87–95. DOI: 10.6060/ivkkt.20256811.7165.

INTRODUTION

Zinc-air battery, also known as zinc-oxygen-air battery, is an environmentally friendly battery with many advantages such as small size, small mass, large charge, safety and reliability, and can maintain normal operation in a wide temperature range without corrosion [1-2]. When discharging, zinc loses electrons and oxidizes, electrons flow to the positive electrode through the outer electrode, the oxygen molecule adsorbed on the catalyst obtains electrons, and then the O=O bond breaks at the catalyst/gas interface, and the reduction product is transferred to the negative electrode through the electrolyte after deattachment, and the total reaction is Zn and oxygen to produce ZnO.

Although noble metal catalysts have achieved superior performance in fuel cell cathode oxygen reduction electrode reactions, the scarcity, cost and low durability of these metal catalysts make it difficult to carry out large-scale applications [3-5]. Pt/C catalyst is an oxygen reduction reaction catalyst based on metal platinum nanoparticles (Pt NPs) loaded on carbon, and only platinum atoms on the surface of Pt NPs participate in the reaction [6]. Therefore, reducing the size of Pt NPs to the single-atom scale represents the best way to maximize the utilization of Pt [7-9]. As the most commonly used cathodic oxygen reduction catalyst among all pure metal catalysts, the oxygen reduction activity of Pt is mainly affected by the crystallinity, morphology and size. For example, the oxygen reduc-

tion activity of Pt (100) is much higher than that of Pt (111) due to the different adsorption rate of sulfuric acid in sulfuric acid medium. The performance of catalyst can be effectively improved by controlling the shape and form of platinum. By dispersing platinum on the gold nanorods, this hybrid electrocatalyst greatly reduces the amount of platinum and shows extremely high ORR high activity to oxygen reduction reactions (ORR) [10].

Wang et al. [11] prepared ordered and vertically arranged Pt nanotubes by template method. Pt nanotubes are composed of highly dispersed platinum nanoparticles with an average thickness of about 15nm, and their catalytic activity is greatly improved. In order to overcome the limitations of precious metals, researchers are increasingly focusing on alloying precious metals with transition metals (such as Ni, Co, Mn, Fe) and other precious metals (such as Rh, Ru, Pd, Au, Ag) when designing and synthesizing catalysts. Studies have shown that Pt-Pd alloy and $PtNi_3$ alloy catalysts with core-shell structure show unprecedented catalytic activity and stability, which provides a beneficial exploration for the selection of bimetallic oxygen reduction catalysts with low platinum content [12-13]. Ternary metal alloys, such as PT-Co-Cu, also show superior catalytic activity and are expected to replace simple Pt oxygen reduction catalysts. In addition to Pt, other Pt group precious metals include Ruthenium (Ru) [14], Iridium (Ir) [15], etc., and non-Pt group precious metals such as silver (Ag) [16], etc., which can also exhibit high ORR activity due to its adsorption and desorption energy to oxygen-containing species similar to Pt. At present, the design focus of noble metal oxygen reduction catalyst has changed from single precious metal to noble metal alloy and non-noble metal catalyst, which provides important technical support for promoting the sustainable development of oxygen reduction reaction in the field of energy.

As a catalyst, platinum (Pt) is limited by its scarcity, high price and instability in the reaction process. Platinum-based catalysts usually do not have tolerance to alcohols, and the resulting toxic CO tends to occupy the active site, resulting in decreased performance and mixing potential problems. Therefore, the search for alternative materials that can reduce or completely replace the precious metal platinum as oxygen reduction catalyst is an important research direction in the field of chemistry and materials science. At present, it mainly focuses on the non-precious metals represented by transition metal oxides, nitrogen-doped carbon materials containing transition metals, and completely nonmetallic heteratomic-doped carbon materials. Transition metal oxides, which typically contain elements such as iron, cobalt, and nickel, are much cheaper than platinum and are abundant. By changing their surface structure and composition, these oxides can optimize their activity for oxygen reduction reaction (ORR). Nitrogen-doped carbon materials containing transition metals can also exhibit good oxygen reduction activity, and in these materials, the introduction of nitrogen atoms can create active sites and enhance the electron conductivity of the material, thereby improving its catalytic performance. Due to the cheapness and availability of carbon-based materials, these materials have significant advantages in terms of cost. Among them, metal carbides, such as tungsten carbide and iron carbide, have been intensively studied in oxygen reduction reaction (ORR) and hydrogen evolution reaction (HER) due to their excellent electrical conductivity and unique electronic structure [17,18]. Metal nitrides are a special class of compounds that are composed of transition metal elements and nitrogen. These compounds have many unique physical and chemical properties, including high hardness, high melting point and good electrical conductivity, and the main advantage is their stability. Under high temperature and high potential conditions, these catalysts are not susceptible to corrosion and can maintain stable catalytic performance. In addition, nitrogen is easily embedded in the vacancy of the transition metal and does not cause significant changes in the crystal, which helps to improve the D-band structure of the catalyst and reduce the Fermi level of the transition metal, thereby improving the catalytic performance of metal oxides (such as CoO, MnO_2, etc.) as catalytic materials are easy to prepare, and show good stability in alkaline or oxidizing media. However, due to its poor electrical conductivity, its activity in the catalytic process is somewhat limited [19].

Transition metal composite nitrogen-doped carbon materials (M-N-C, M=Mn, Fe, Co, Ni, etc.) have been widely studied, and their active site is usually M-NX. The research of such materials dates back to 1964 when Jasinski et al. [20] found that cobalt phthalocyanine can also catalyze the reaction of oxygen in alkaline electrolyte, and this nitrogen-doped carbon-supported single atom catalyst can further improve the catalytic efficiency and atomic utilization, and improve the selectivity through the metal-carrier interface. Therefore, nitrogen-doped carbon supported single atom catalyst has the advantages of low cost, good stability, friendly environment and easy to obtain, and is expected to become a potential new catalyst. The realization of efficient ORR reaction is of great significance for promoting the commercial application of a new generation of green energy conversion devices

such as fuel cells, and atomically dispersed transition metal-nitrogen-doped carbon-based materials show great application potential in the field of ORR catalysis due to their multiple advantages such as high intrinsic activity, atomic utilization rate and clear active site [21].

In view of the above research hotspots, this paper develops a new catalyst by loading hemoglobin (Hb) and carbon trinitrogen (g-C_3N_4) on porous carbon materials to reduce costs and improve stability, and improves the structure and performance of electrocatalysts by means of material engineering, so as to achieve a more efficient and environmentally friendly energy conversion system to meet the future needs of society for sustainable energy.

EXPERIMENTAL PART

1. *Preparation method of catalyst*

1 mg of catalyst was weighed and dissolved into a mixture of 20 isopropyl alcohol and 160 L ultra-pure water, then 5 wt.% 20 μl of naphthol solution was added, ultrasonic dispersion was carried out for 30 min, and 15 μl of ink solution drops were removed onto a clean surface of a glassy carbon electrode. The catalyst thin film electrode with a load of 0.196 mg·cm^{-2} was prepared by natural drying at room temperature. Then the electrodes were dried at room temperature, and CV curves and LSV curves were measured at an electrochemical workstation Pre-oxidized carbon black (OCB) synthesis: First, 0.2 g BP2000 carbon black was added to 50 ml beeper, and 30 ml 6 mol/L HNO_3 was ultrasonically added to form a uniform suspension, and then the mixture was magnetically stirred at 70 °C for 12 h. Finally, the carbon black was filtered after pre-oxidation and washed and dried in sufficient ultra-pure water for use.

G-C_3N_4 synthesis: 10 g melamine was placed in a corundum crucible with a lid at 5 °C/min to 550 °C and held for 4 h to obtain G-C_3N_4 yellow powder.

(1) OCB-Hb@g-C_3N_4 catalyst: 50 mg OCB and X mg (X = 50, 100, 150) Hb were added to 30 ml ultra-pure water to form a uniform suspension. The mixture was then magnetically stirred at 300 rpm at 25 °C for 12 h and then steamed in a vacuum drying oven at 80 °C. 100 mg of dried OCB-Hb and 240 mg of g-C_3N_4 were ground in agate body for 0.5 h. The obtained powder was pyrolyzed at a high temperature under Ar at a pyrolysis rate of 5 °C/min, held at 350 °C for 2 h, and at 900 °C for 2 h. The resulting product was acid-washed in 0.5M H_2SO_4 solution at 80 °C for 10 h to remove metal oxides, and dried in a vacuum drying oven at 60 °C.

(2) CB-HB@g-C_3N_4 catalyst: CB-Hb@g-C_3N_4 catalyst type is in the OCB-Hb@g-C_3N_4 step, CB is carbon black that has not been treated by 6 mol/L HNO_3.

(3) CB@g-C_3N_4 catalyst: CB@g-C_3N_4 The catalyst is similar to the CB-Hb@g-C_3N_4 step, except hemoglobin is not added.

2. *Preparation method of membrane electrode*.

A quantity of 1 mg catalyst is weighed out and dissolved into a mixed solution containing 20 (specify units, such as μL/mL) isopropyl alcohol and 160 L ultra-pure water. After that, 20 μL of 5 wt% naphthol solution is introduced into the system, and the mixture is subjected to ultrasonic dispersion for 30 min. Subsequently, 15 μL of the resulting ink solution is pipetted and deposited onto the surface of a pre-cleaned glassy carbon electrode. The catalyst thin film electrode with a load of 0.196 mg·cm^{-2} was prepared by natural drying at room temperature. Then the electrodes were dried at room temperature, and CV curves and LSV curves were measured at an electrochemical workstation.

RESULTS AND DISCUSSION

1. *Characterization of physical and chemical properties of carbon black*

Field emission scanning electron microscopy (SEM) was used to study the influence of the morphology and structure of carbon black BP2000 on the non-pre-oxidation and pre-oxidation respectively, as shown in Fig. 1(a) and (b). Fig. 1(a) shows the microscopic morphology of carbon black BP2000. Due to its special nanoscale branched chain structure, carbon black BP2000 not only has high electrical conductivity, but also ensures that active substances can be effectively packed tightly in it. This loose porous property allows it to hold more active substances, which is crucial for improving the performance of the catalyst, especially in terms of increasing the current density of the catalyst and the battery capacity. It can be seen from Fig. 1(b) that the carbon black BP2000 obtained after pre-oxidation treatment does not agglomerate, and the dispersion is very uniform. The pre-oxidized carbon black BP2000 was also subjected to a BET test (MikeTriStarII3020 N_2), and the results are shown in Table 1, further demonstrating its porous properties.

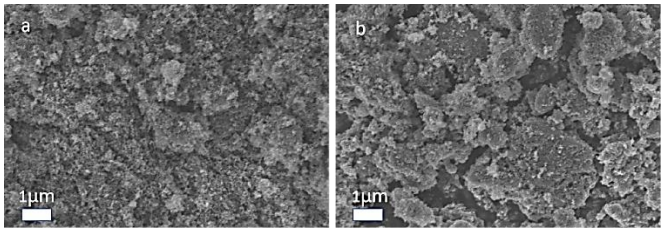

Fig. 1: SEM image of carbon black BP2000 (a) without pre-oxidation; (b) SEM image of pre-oxidation

Рис. 1. СЭМ-изображение технического углерода BP2000 (a) без предварительного окисления; (b) СЭМ-изображение с предварительным окислением

Table 1

Textural properties of BP2000 after pre-oxidation

Таблица 1. **Текстурные свойства BP2000 после предварительного окисления**

Sample	SBET (m^2/g)	Total pore volume (cm^3/g)	Micropores volume (cm^3/g)	Mesopores volume (cm^3/g)
BP2000 after pre-oxidation	1458	2.05	0.24	1.81

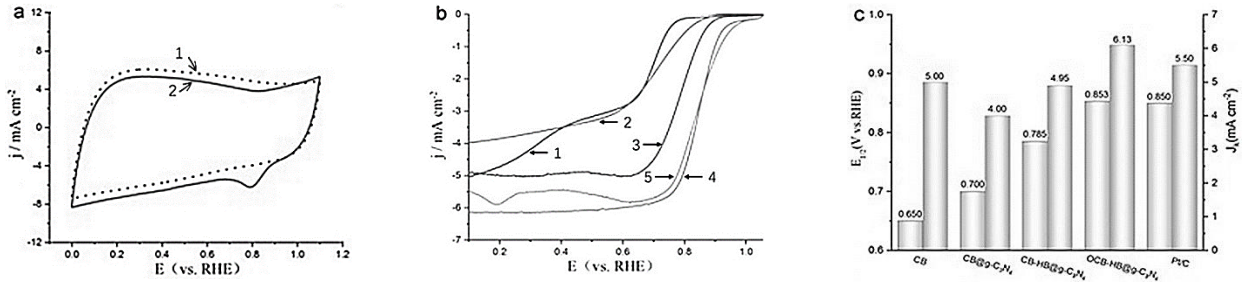

Fig. 2. (a) curve 1: CV curve of OCB-HB@g-C_3N_4 catalyst in 0.1mol/L KOH electrolyte saturated with N_2 , curve 2: CV curve of OCB-HB@g-C_3N_4 catalyst in 0.1mol/L KOH electrolyte saturated with O_2 ; (b) Curves 1, 2, 3, 4, and 5 correspond to the LSV curves of CB, CB@g-C_3N_4, CB-HB@g-C_3N_4, OCB-HB@g-C_3N_4, and Pt/C catalysts in O_2-saturated 0.1mol/L KOH electrolyte ; (c) Histogram of half wave potential and limit current density of catalysts with different contrast samples

Рис. 2. (a) кривая 1: циклическая вольтамперная (ЦВ) кривая катализатора OCB-HB@g-C_3N_4 в электролите 0,1 моль/л KOH, насыщенном N_2; кривая 2: циклическая вольтамперная (ЦВ) кривая катализатора OCB-HB@g-C_3N_4 в электролите 0,1 моль/л KOH, насыщенном O_2; (b) кривые 1, 2, 3, 4 и 5 соответствуют линейно-сканировочным вольтамперным (ЛСВ) кривым катализаторов CB, CB@g-C_3N_4, CB-HB@g-C_3N_4, OCB-HB@g-C_3N_4 и Pt/C в электролите 0,1 моль/л KOH, насыщенном O_2; (c) гистограмма полуволтного потенциала и предельной плотности тока катализаторов с различными контрольными образцами

2. *Catalyst kinetic process test*

The electrochemical test was carried out on the CHI 760E electrochemical workstation with 0.1M KOH solution as electrolyte, 100 mL/min oxygen flow, graphite rod as auxiliary electrode and Hg/HgO as reference electrode. Cyclic voltammetry (CV) tests were performed in a 0.1 M KOH solution saturated with N_2 or O_2 at a scan rate of 50 mV/s. Linear sweep voltammetry (LSV) is performed at 1600 rpm from 0 V to 1.1 V at a scan rate of 10 mV/s. The H_2O_2 % and the number of transferred electrons (n) of the catalyst in ORR are calculated by formulas (1.1) and (1.2):

$$H_2O_2(\%) = 200 \cdot \frac{I_R/N}{(I_R/N) + I_D} \quad (1.1)$$

$$n = 4 \cdot \frac{I_D}{(I_R/N) + I_D} \quad (1.2)$$

Where I_R and I_D are ring current and disk current respectively, the current collection efficiency of N is 0.38.

The K-L equation is:

$$\frac{1}{J} = \frac{1}{J_k} + \frac{1}{J_l} = \frac{1}{J_k} + \frac{1}{Bw^{1/2}} \quad (1.3)$$

$$B = 0.2nFC_0\, D_0^{2/3} v^{-1/6} \quad (1.4)$$

Where J is the current density value measured during the experiment; J_k is the kinetic current density obtained by calculation; J_l is the limit current density obtained during experimental testing; ω is the angular velocity obtained by converting the rotation speed of the selected disk electrode; n is the calculated number of electrons transferred in the ORR process. F is the Faraday coefficient (96485 C/mol); The actual concentration of the reactants provided during the experimental test ($1.2 \cdot 10^{-6}$ mol/cm); Is the diffusion parameter of reactant O_2 during ORR process ($1.9 \cdot 10^{-5}$ cm^2/s); v is the viscosity parameter of solution in ORR (0.01 cm^2/s).

3. *Oxygen reduction performance test*

Fig. 2(a) shows the catalyst OCB-HB@g-C_3N_4 using a rotating disk electrode (RDE) to perform cyclic voltammetry test in 0.1M KOH solution saturated with O_2 and N_2. As shown in the figure, there is no reduction peak in the cyclic voltammetry curve under N_2 saturation state, while under O_2 saturation state, there is a reduction peak in the cyclic voltammetry curve. The cyclic voltammetry curve shows an obvious reduction peak at 0.80V (vs. RHE), which indicates that the catalyst has good oxygen reduction performance. In order to explore the influence of different preparation conditions on the catalytic performance of the catalyst for oxygen reduction, linear sweep voltammetry tests were performed at 1600 rpm in 0.1M KOH electrolyte with saturated oxygen, as shown in Fig. 2(b). CB, CB@g-C_3N_4, CB-HB@g-C_3N_4, OCB-HB@g-C_3N_4 are compared with commercial Pt/C as shown in Fig. 2(c). The half-wave potential and limiting current density of g-C_3N_4 (as a small molecular nitrogen source) and hemoglobin (as an iron source) catalysts are much higher than those of commercial carbon black BP2000, indicating that these two substances play an important role in improving the catalytic activity of carbon black.

The optimal sample OCB-HB@g-C_3N_4 has a half-wave potential of 0.853V (vs. RHE) that is similar to the commercial Pt/C half-wave unit of 0.850V (vs. RHE), but the limiting current density is much higher than that of commercial Pt/C, as shown in Table 2. It is speculated that the reasons are as follows: firstly, after the cheap BP2000 carbon black is treated with high concentration nitric acid, its surface is enriched with oxygen-containing functional groups such as hydroxyl carboxyl groups. These oxygen-containing functional groups will act as metal anchoring sites to capture more metals, thus improving the oxygen reduction performance of the catalyst. [22] Secondly, the BP2000 carbon black adsorbed with hemoglobin is ground with g-C_3N_4. As a small molecular nitrogen source, g-C_3N_4 can first physically block the aggregation of hemoglobin in space, and secondly, more importantly, it can be used to capture Fe atoms in the migration process during pyrolysis to prevent a large loss of Fe atoms.

Table 2

Comparison of ORR properties of OCB-Hb@g-C_3N_4 catalyst with other non-precious metal catalysts
***Таблица 2*. Сравнение свойств ORR катализатора OCB-Hb@g-C_3N_4 с другими катализаторами на основе недрагоценных металлов**

Catalysts	$E_{1/2}$(V)	J_L(mA/cm^2)	Mass loading(mg/cm^2)	References
CoFe@NC-SE	0.82	6.25	0.25	[23]
NiCo-N-TC-H	0.80	5.94	-	[24]
$Co_{0.25}Ni_{0.75}$@NCNT30	0.84	-	0.6	[25]
MnO-Co@NC	0.75	5.90	0.5	[26]
Fe-NCCs	0.82	-	0.1	[27]
Bi-CoP/NP-DG	0.81	-	-	[28]
In-CoO/CoPFNS	0.81	-	-	[29]
HNCSs	0.82	5.48	0.2	[30]
DAC-N800	0.79	6.17	-	[31]
CoNC@$CoFeS_2$	0.80	-	0.35	[32]
NMC-1	0.82	4.50	-	[33]
Pt/C	0.85	5.80	0.384	This Work
OCB@HB-g-C_3N_4	0.853	6.13	0.384	This Work

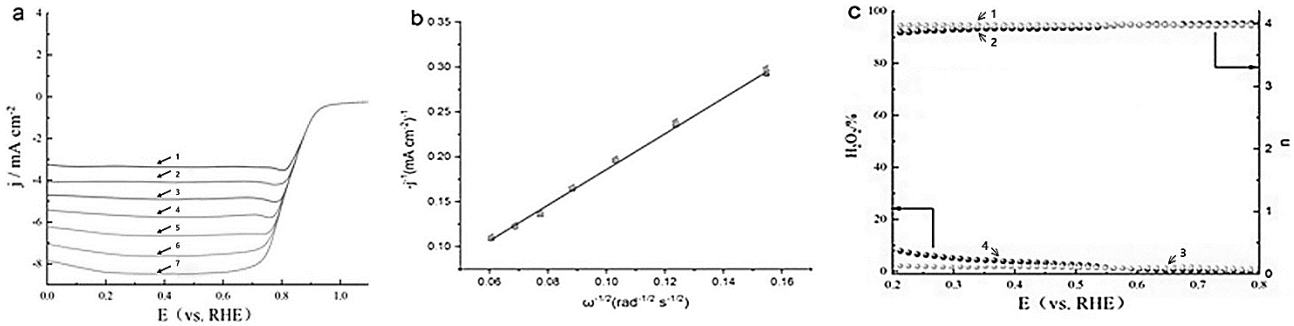

Fig. 3. (a) Curves 1, 2, 3, 4, 5, 6 and 7 correspond to the LSV curves of OCB-HB@g-C_3N_4 catalyst at 400, 625, 900, 1225, 1600, 2025, 2500 rpm ; (b) KL diagram of OCB-HB@g-C_3N_4 catalyst at different potentials; (c) Curves 1and 2 correspond to the electron transfer number of OCB-HB@g-C_3N_4 catalyst and Pt/C, Curves 3and 4 correspond to H_2O_2 yield of OCB-HB@g-C_3N_4 catalyst and Pt/C
Рис. 3. (a) кривые 1, 2, 3, 4, 5, 6 и 7 соответствуют линейно-сканировочным вольтамперным (ЛСВ) кривым катализатора OCB-HB@g-C_3N_4 при скоростях вращения 400, 625, 900, 1225, 1600, 2025 и 2500 об/мин; (b) диаграмма К-Л (Куттлера-Лэнгмюра) катализатора OCB-HB@g-C_3N_4 при различных потенциалах; (c) кривые 1 и 2 соответствуют числу переносимых электронов катализаторов OCB-HB@g-C_3N_4 и Pt/C; кривые 3 и 4 соответствуют выходу пероксида водорода (H_2O_2) катализаторов OCB-HB@g-C_3N_4 и Pt/C

In order to further study the ORR reaction kinetics on the catalyst, LSV at OCB-HB@g-C_3N_4 at different speeds of 400-2500 rpm was measured. As shown in Fig. 3(a), the limiting current density increases with the increase of rotational speed because, to a certain extent, the higher the rotational speed, the shorter the diffusion distance. According to the limit current density and voltage, the LSV curves at different speed are drawn. It is found that the limit current density has a linear relationship with the speed in the range of 0.35V to 0.6V. Correspondingly, Fig. 3(b) shows that the polarization curve of the catalyst at different sweep speeds has good linearity and normalization, the potential range is 0.35V to 0.60V, and the electron

transfer number is 3.75. In addition, the hydrogen peroxide yield and electron transfer number during ORR were measured with a rotating ring disk device (RRDE), as shown in Fig. 3(c). The H_2O_2 yield of OCB-HB@g-C_3N_4 is about 7%, which is slightly higher than that of Pt/C. According to the formula, the electron transfer number of OCB-HB@g-C_3N_4 is between 3.72 and 3.78. Based on the above data, it can be seen that OCB-HB@g-C_3N_4 is nearly four electron reaction paths.

In addition, the electrochemical active region is analyzed by scanning rate and non-Faraday current slope in cyclic voltammetry, and the Cdl of the optimal sample OCB-HB@g-C_3N_4 is calculated. According to relevant literature reports, the larger the electrochemical double layer capacitance, the larger the effective surface area of the catalyst for catalytic reaction, and the higher the catalytic activity of ORR.

Fig. 4(a) shows CV curves drawn at different scanning speeds. The electrocatalytic active area is characterized by the fitting of scanning rates of different CV with non-Faraday current slopes. As shown in Fig. 4(b), the prepared catalyst double layer capacitance (Cdl) of 54.2 mF/cm^2 was fitted. The catalytic active area is relatively large, indicating that the optimal OCB-HB@g-C_3N_4 catalyst has better oxygen reduction performance.

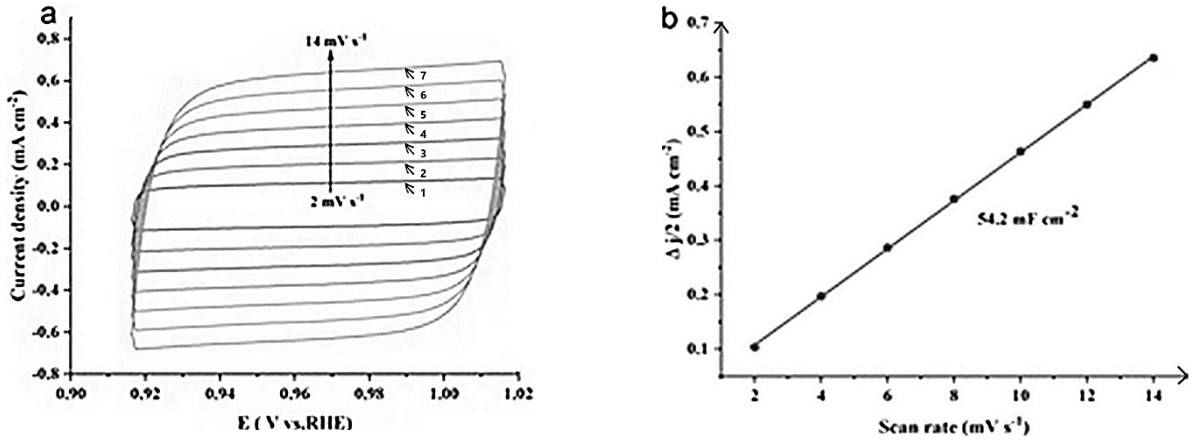

Fig. 4. (a) Curves 1, 2, 3, 4, 5, 6, and 7 correspond to the CV curve of OCB-HB@g-C_3N_4 catalyst in the non-Faraday potential range at the scan rate of 2, 4, 6, 8, 10, 12, 14 mV s-1; (b) Double layer capacitance of OCB-HB@g-C_3N_4 catalyst

Рис. 4. (a) кривые 1, 2, 3, 4, 5, 6 и 7 соответствуют циклическим вольтамперным (ЦВ) кривым катализатора OCB-HB@g-C_3N_4 в диапазоне нефарадеевских потенциалов при скорости сканирования 2, 4, 6, 8, 10, 12, 14 мВ/с; (b) двойной слой ёмкости катализатора OCB-HB@g-C_3N_4

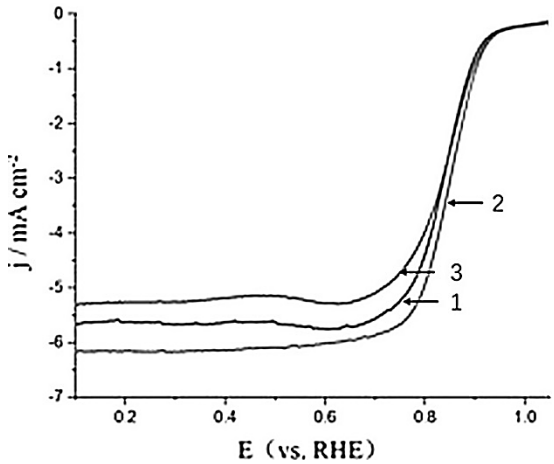

Fig. 5. Curves 1, 2, and 3 correspond to the linear sweep voltammetry (LSV) curves of the OCB-HB@g-C_3N_4 catalysts prepared with hemoglobin contents of 50, 100, and 150 mg, respectively

Рис. 5. Кривые 1, 2 и 3 соответствуют линейно-сканировочным вольтамперным (ЛСВ) кривым катализаторов OCB-HB@g-C_3N_4, приготовленных при содержании гемоглобина 50, 100 и 150 мг соответственно

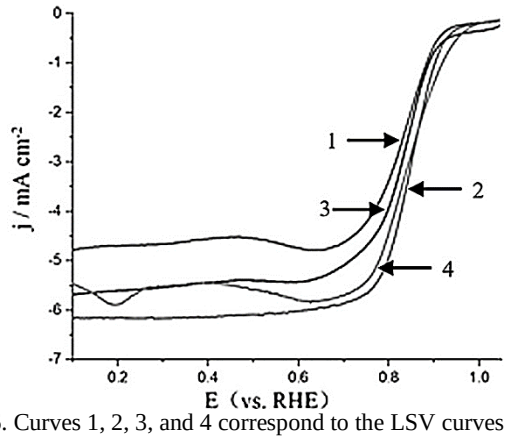

Fig. 6. Curves 1, 2, 3, and 4 correspond to the LSV curves of the OCB-HB@g-C_3N_4 catalysts (prepared at pyrolysis temperatures of 800, 900, and 1000 °C) and the Pt/C catalyst in O_2-saturated 0.1mol/L KOH electrolyte, respectively

Рис. 6. Кривые 1, 2, 3 и 4 соответствуют линейно-сканировочным вольтамперным (ЛСВ) кривым катализаторов OCB-HB@g-C_3N_4 (приготовленных при температурах пиролиза 800, 900 и 1000 °C) и катализатора Pt/C в электролите 1 моль/л KOH, насыщенном кислородом (O_2), соответственно

4. *Effects of different hemoglobin contents on catalyst ORR*

In order to study the effect of hemoglobin content on catalytic activity, ORR activity of catalysts synthesized with different hemoglobin content was tested in 0.1 mol/L KOH solution saturated with O_2 (Fig. 5). According to LSV, there is a corrected half-wave potential of 0.853V (vs. RHE) and a greater limiting current density of 6.13 mA cm^{-2} when the hemoglobin supplemental level is 100 mg. The reason for this is that the addition of too much metal may lack the corresponding binding site with carbon black, resulting in metal agglomeration and pore structure blockage in the pyrolysis process, thus reducing the activity of the catalyst.

5. *Influence of different pyrolysis temperatures on catalyst ORR*

In order to study the effect of pyrolysis temperature on catalytic activity, ORR activity of the synthesized catalyst was tested in 0.1 mol/L KOH solution saturated with O_2 at different temperatures (800, 900, 1000 °C) (Fig. 6). The half-wave potential of OCB-HB@g-C_3N_4 obtained at 900 °C is 0.853V, which is higher than that of OCB-HB-1000@g-C_3N_4 (0.832V) and OCB-HB-800@g-C_3N_4 (0.835V), indicating that the best ORR performance can be obtained by heat treatment at 900 °C. The results show that temperature can promote the increase of active N species, but too high temperature will lead to the conversion of active N to inactive N species, thus reducing the catalytic performance.

CONCLUSION

In this paper, aimed at solving a number of problems such as low activity and poor stability of oxygen reduction electrocatalyst for iron-doped carbon materials, an experimental study was conducted on the change in the electronic structure of the material by doping with hemoglobin. Also, the electrocatalytic activity of oxygen reduction and the stability of the OCB-HB@g-C_3N_4 catalyst were systematically analyzed, as well as ways to improve and enhance the performance of the catalyst.) Through the analysis and comparison of the experimental data, the catalytic performance at 900 °C is better than that at 800 °C and 1000 °C. The catalytic efficiency of hemoglobin at a concentration of 100 mg was better than at a concentration of 50 mg and 150 mg. The ORR performance of the catalyst can be improved by changing temperature, pre-oxidizing carbon black, adding hemoglobin, adding carbon triazene and using different types of carbon black. These findings provide new ideas for the development of catalysts for oxygen reduction reaction (ORR) of cathode core reaction in energy conversion devices such as zinc-air batteries.

Авторы заявляют об отсутствии конфликта интересов, требующего раскрытия в данной статье.

The authors declare the absence of a conflict of interest warranting disclosure in this article.

ЛИТЕРАТУРА
REFERENCES

1. **Liu J.N, Zhao C.X., Wang J.** A brief history of zinc–air batteries: 140 years of epic adventures. *Energy Environ. Sci.* 2022. V. 15. N 11. P. 4542-4553. DOI: 10.1039/D2EE02440C.
2. **Wang Q., Kaushik S., Xiao X.** Sustainable zinc–air battery chemistry: advances, challenges and prospects. *Chem. Soc. Rev.* 2023. V. 52. N 17. P. 6139-6190. DOI: 10.1039/D2CS00684G.
3. **Saikawa K., Nakamura M., Hoshi N.** Structural effects on the enhancement of ORR activity on Pt single-crystal electrodes modified with alkylamines. *Electrochem. Commun.* 2017. V. 87. P. 5-8. DOI:10.1016/j. elecom2017.12.016.
4. **Khaskov M.A.** Thermoporometry and oxyreactive thermal analysis for study of carbon matrices. *ChemChemTech [Izv. Vyssh. Uchebn. Zaved. Khim. Khim. Tekhnol.]*. 2023. V. 66. N 10. P. 24-31 (in Russian). **Хасков М.А.** Термопорометрия и окислительный термический анализ при исследовании углеродных матриц. *Изв. вузов. Химия и хим. технология.* 2023. Т. 66. Вып. 10. С. 24-31. DOI: 10.6060/ivkkt.20236610.1y.
5. **Sakhibgareev S.R., Tsadkin M.A., Badikova A.D., Gumerova E.F.** Catalysts for destruction of hydrocarbon raw materials based on barium chloride. *ChemChemTech [Izv. Vyssh. Uchebn. Zaved. Khim. Khim. Tekhnol.]*. 2022. V. 65. N 9. P. 64-73 (in Russian**). Сахибгареев С.Р., Цадкин М.А., Бадикова А.Д., Гумерова Э.Ф.** Катализаторы деструкции углеводородного сырья на основе хлорида бария. *Изв. вузов. Химия и хим. технология.* 2022. Т. 65. Вып. 9. С. 64-73. DOI: 10.6060/ivkkt.20226509.6535.
6. **Wagner F., Gasteiger H., Makharia R.** Catalyst development needs and pathways for automotive pem fuel cells. *ECS Transact.* 2006. V. 3. N 1. P. 19-29. DOI: 10.1149/1.2356119.
7. **Zhang L., Roling L.T., Wang X.** Platinum-based nanocages with subnanometer-thick walls and well-defined, controllable facets. *Science.* 2015. V. 349. (6246). P. 412-416. DOI: 10.1126/science. aab0801.
8. **Liu J.** Catalysis by Supported Single Metal Atoms. *ACS Catalysis.* 2016. V. 7. N 1. P. 34-59. DOI: 10.1021/acscatal.6b01534.
9. **Zhu C., Fu S., Shi Q.** Single - atom electrocatalysts. *Angew. Chem. Int. Ed.* 2017. V. 56. N 45. P. 13944-13960. DOI: 10.1002/anie.201703864.
10. **Zhong X., Yu H.Y., Wang X.D.** Pt@Au nanorods uniformly decorated on pyridyne cycloaddition graphene as a highly effective electrocatalyst for oxygen reduction. *ACS Appl. Mater. Interfaces.* 2014. V. 6. N 16. P. 13448-13454. DOI: 10.1021/am5020452.
11. **Wang G., Lei L., Jiang J.** An ordered structured cathode based on vertically aligned Pt nanotubes for ultra-low Pt loading passive direct methanol fuel cells. *Electrochim. Acta.* 2017. V. 252. P. 541-548. DOI: 10.1016/j.electacta.2017.08.1.
12. **Aoki N., Inoue H., Shirai A.** Electrochemical and Chemical Treatment Methods for Enhancement of Oxygen Reduction Reaction Activity of Pt Shell-Pd Core Structured Catalyst. *Electrochim. Acta.* 2017. V. 17. P. 31-37. DOI: 10.1016/j.electacta.2017.05.054.
13. **Gan L., Rudi S., Cui C.** Size-Controlled Synthesis of Sub-10 nm $PtNi_3$ Alloy Nanoparticles and their Unusual Volcano-

Shaped Size Effect on ORR Electrocatalysis. *Small*. 2016. V. 12. P. 3189-3196. DOI: 10.1002/smll.201600027.
14. **Xiao M, Gao L., Wang Y.** Engineering energy level of metal center: Ru single-atom site for efficient and durable oxygen reduction catalysis. *J. of the Am. Chem. Soc.* 2019. V. 141. N 50. P. 19800-19806. DOI: 10.1021/jacs.9b09234.
15. **Xiao M., Zhu J., Li G.** A single-atom iridium heterogeneous catalyst in oxygen reduction reaction. *Angew. Chem. Int. Ed.* 2019. V. 58 N 28. P. 9640-9645. DOI: 10.1002/anie.201905241.
16. **Sui R., Zhang X., Wang X.** Silver based single atom catalyst with heteroatom coordination environment as high performance oxygen reduction reaction catalyst. *Nano Res.* 2022. V. 15. N 9. P. 7968-7975. DOI: 10.1007/s12274-022-4499-8.
17. **Sui S., Wang X., Zhou X.** A comprehensive review of Pt electrocatalysts for the oxygen reduction reaction: Nanostructure, activity, mechanism and carbon support in PEM fuel cells. *J. Mater. Chem. A.* 2017. V. 5. DOI: 10.1039/C6TA08580F.
18. **Bhatt M.D., Lee G., Lee J.S.** Screening of Oxygen-Reduction-Reaction-Efficient Electrocatalysts Based on Ag–M (M = 3d, 4d, and 5d Transition Metals) Nanoalloys: A Density Functional Theory Study. *Energy Fuels.* 2017. V. 31. P. 1874-1881. DOI: 10.1021/acs.energyfuels.6b02991.
19. **Zhao Y., Wang H., Li J.** Regulating the Spin-State of Rare-Earth Ce Single Atom Catalyst for Boosted Oxygen Reduction in Neutral Medium. *Adv. Funct. Mater.* 2023. V. 33. N 47. P. 2305268. DOI: 10.1002/adem.202305268.
20. **Jasinski R.** A new fuel cell cathode catalyst. *Nature*. 1964. V. 201. P. 1212-1213. DOI: 10.1038/2011212a0.
21. **Xu H., Wang D., Yang P.X.** A theoretical study of atomically dispersed MN_4/C (M = Fe or Mn) as a high-activity catalyst for the oxygen reduction reaction. *Phys. Chem. Chem. Phys.* 2020. V. 22. P. 28297-28303. DOI: 10.1039/d0cp04676k.
22. **Duarte M.F.P., Rocha I.M.., Figueiredo J.L.** CoMn-LDH@carbon nanotube composites: Bifunctional electrocatalysts for oxygen reactions. *Catal. Today.* 2018. V. 301. P. 17-24. DOI: 10.1016/j.cattod.2017.03.046.
23. **Samanta A., Raj C.R.** Bifunctional nitrogen-doped hybrid catalyst based on onion-like carbon and graphitic carbon encapsulated transition metal alloy nanostructure for rechargeable zinc-air battery. *J. Power Sources.* 2020. V. 455. P. 227975. DOI: 10.1016/j.jpowsour.2020.227.
24. **Samanta A., Ghatak A., Bhattacharyya S.** Transition metal alloy integrated tubular carbon hybrid nanostructure for bifunctional oxygen electrocatalysis. *Electrochim. Acta.* 2020. V. 348. P. 136274. DOI: 10.1016/j.electacta 2020.136274.
25. **Kundu A., Samanta A., Raj C.R.** Hierarchical Hollow MOF-Derived Bamboo-like N-doped Carbon Nanotube-Encapsulated Co0 .25Ni 0.75 Alloy: An Efficient Bifunctional Oxygen Electrocatalyst for Zinc-Air Battery. *ACS Appl. Mater. Interfaces.* 2021. V. 13. N 26. P. 30486-30496. DOI: 10.1021/acsami.1c01875.
26. **Samanta A., Barman B.K., Mallick S.** Three-Dimensional Nitrogen-Doped Graphitic Carbon-Encapsulated MnO-Co Heterostructure: A Bifunctional Energy Storage Material for Zn-Ion and Zn-Air Batteries. *ACS Appl. Energy Mater.* 2020. V. 3. N 10. P. 10108-10118. DOI: 10.1021/acsam.0c01811.
27. **Jia N., Xu Q., Zhao F.** Fe/N Codoped Carbon Nanocages with Single-Atom Feature as Efficient Oxygen Reduction Reaction Electrocatalyst. *ACS Appl. Energy Mater.* 2018. V. 1. N 9. P. 4982-4990. DOI: 10.1021/acsaem.8b00970.
28. **Chen J., Ni B., Hu J.** Defective graphene aerogel-supported Bi-CoP nanoparticles as a high-potential air cathode for rechargeable Zn-air batteries. *J. Mater. Chem. A.* 2019. V. 7. N 39. P. 22507-22513. DOI: 10.1039/C9TA07669G.
29. **Jin W., Chen J., Liu B.** Oxygen Vacancy-Rich In-Doped CoO/CoP Heterostructure as an Effective Air Cathode for Rechargeable Zn-Air Batteries. *Small*. 2019. V. 15. N 46. e1904210. DOI: 10.1002/smll.201904210.
30. **Chai L, Zhang L., Wang X.** Bottom-up synthesis of MOF-derived hollow N-doped carbon materials for enhanced ORR performance. *Carbon*. 2019. V. 146. P. 248-256. DOI: 10.1016/j.carbon.2019.02.00.
31. **Qiu Y., Ali S., Lan G.** Defect-rich activated carbons as active and stable metal-free catalyst for acetylene hydrochlorination. *Carbon*. 2019. V. 146. P. 406-412. DOI: 10.1016/j.carbon.2019.01.102.
32. **Wang Y., Jin W., Xuan C.** In-situ growth of $CoFeS_2$ on metal-organic frameworks-derived Co-NC polyhedron enables high-performance oxygen electrocatalysis for rechargeable zinc-air batteries. *J. Power Sources.* 2021. V. 512. P. 230430. DOI: 10.1016/j.jpowsour.2021.230430.
33. **Li X., Zhao Y., Yang Y.** A universal strategy for carbon-based ORR-active electrocatalyst: One porogen, two pore-creating mechanisms, three pore types. *Nano Energy.* 2019. V. 62. P. 628-637. DOI: 10.1016/j.nanoen.2019.05.

Поступила в редакцию 11.11.2024
Принята к опубликованию 13.05.2025

Received 11.11.2024
Accepted 13.05.2025